

# Supramolecular Assembly and Interfacial Hydration of Tandem Repeat Dipeptides on 2D Nanomaterials: Insights From 3D-AFM Measurements and MD Simulations

Ayhan Yurtsever, \* Fabio Priante, Linhao Sun, \* Marie Sugiyama, Kazuki Miyata, Keisuke Miyazawa, Sanhanut Kesornsit, Katsuhiro Maeda, Adam S. Foster, Yuhei Hayamizu,\* Mehmet Sarikaya, and Takeshi Fukuma\*

The design of functional bionanomaterials formed by peptide supramolecular organizations on atomically-thick solids relies on understanding molecular self-assembly mechanisms. This study investigates the structural aspects of short peptide assemblies on 2D crystallographic solid surfaces, aiming to create structurally well-defined peptide-solid hybrid systems with soft interfaces. The understanding of complex interplay between sequence-specific molecular interactions among peptides and substrates toward controlled nanoarchitecture formation remains challenging. The lack of understanding of the role of local hydration structures at the molecular level further hinders the rational design and functional control of these systems. A custom-built atomic force microscope, complemented by molecular dynamics simulations, is used to study the assembly of Tyr-His (YH) dipeptides with tandem repeats on cleaved graphite and MoS2 substrates. Molecular visualization of assembled peptide nanostructures and associated localized 3D hydration structures in aqueous solutions demonstrates that the peptides form fully extended, linear conformations aligned with specific crystallographic orientations on the solid substrate. The physical lengths of the assembled peptides match their unfolded states, including the hydration layers. These results underscore the critical role of water in stabilizing and organizing peptide assemblies on solid substrates. This bio/nano system with well-controlled nanoarchitecture offers a highly potent biofunctionalization platform for biomedical and bionanotechnology applications, such as biosensors and bioelectronics.

## 1. Introduction

Short peptides can self-assemble to form supramolecular structures on solid materials, for use as biomolecular substrates to construct functional nanomaterials.[1-3] Peptides are preferable to proteins for surface assemblies due to simpler sequences and ease of manipulation. Recent interest in these biomolecular nanostructures stems from their role in understanding molecular assembly mechanisms relevant to technology, providing a molecular platform for biosensors<sup>[4–6]</sup> and bioelectronics<sup>[1–3,7–11]</sup> applications. By understanding the assembly mechanism,[1,7,12-14] one may design peptide-based materials with tailored structures and desired properties that stem from the nature of the bio/nano soft interfaces, thereby controlling moleculesolid interactions—the key to integrating biology with inorganic materials.[2,15]

Despite significant research, challenges remain in understanding and controlling peptide assembly on solid surfaces, especially regarding the relationship between peptide sequences and self-organized architectures.[16]

A. Yurtsever, L. Sun, K. Miyata, K. Miyazawa, K. Maeda, A. S. Foster,

Nano Life Science Institute (WPI-NanoLSI)

Kanazawa University

Kakuma-machi, Kanazawa 920-1192, Japan E-mail: yurtsever@staff.kanazawa-u.ac.jp;

sunlinhao0502@se.kanazawa-u.ac.jp; fukuma@staff.kanazawa-u.ac.jp



© 2025 The Author(s). Small published by Wiley-VCH GmbH. This is an open access article under the terms of the Creative Commons Attribution-NonCommercial License, which permits use, distribution and reproduction in any medium, provided the original work is properly cited and is not used for commercial purposes.

DOI: 10.1002/smll.202501785

K. Maeda Graduate School of Natural Science and Technology Kanazawa University Kakuma-machi, Kanazawa 920-1192, Japan Graduate School of Frontier Science Initiative Kanazawa University Kakuma-machi, Kanazawa 920-1192, Japan F. Priante, A. S. Foster Department of Applied Physics Aalto University Helsinki 00076, FI, Finland M. Sugiyama, Y. Hayamizu Department of Materials Science and Engineering School of Materials and Chemical Technology

Institute of Science Tokyo Tokyo 152-8550, Japan

E-mail: hayamizu@mct.isct.ac.jp



molecular dynamics (MD) was conducted to understand stabilization and organization on graphite. Our study provides two key insights: i) high-resolution imaging of 3r-, 4r-, and 5r-YH peptide assemblies in water with submolecular spatial resolution, clearly demonstrating linear molecular assembly with single- or twoamino acid resolution; ii) determination of the 3D local hydration structures of water surrounding the peptide assembly structures, emphasizing solvent-peptide interactions critical for stabilizing supramolecular structural ordering. In particular, the dipeptides with varying numbers of YH units(3, 4, and 5) showed peptides forming straight, linear structures aligned with specific crystallographic orientations on the solid surfaces, correlating with their fully extended conformations and specific hydration structures. The role of water in the assembly processes was investigated using 3D-AFM, which provided a detailed view of the 3D molecular organization and the localized hydration structures that enclose the self-organized peptide molecules. The self-organization of simple peptides into predictable crystalline molecular lattices establishing chiral interfaces with the underlying hexagonal surface lattices, such as in graphite and MoS<sub>2</sub>, is highly promising

for integrating biomolecules with solid-state devices. The foun-

dational insights gained from understanding the mechanisms

behind self-assembled peptide nanostructures will drive future

advancements. It is plausible to envision that peptide-2D chalco-

genides, specifically MX2 transition metal dichalcogenides, could

serve as a potential bio/nano hybrid platform for applications in

limitations originate, first, from the use of random peptide sequences on arbitrary solid surfaces without rational design consideration of peptide-solid interactions, which are key to driving the self-assembly processes. Second, there are spatial and temporal limitations in visualizing the formed structures, which require in situ observation in aqueous solutions with molecular or submolecular resolution. Third, the role of solvents in peptide assembly—their local organization around peptide nanostructures and their real-time dynamics—remains poorly understood and largely uncharted at the molecular scale. The solvent-peptide interactions and the resulting solvation/hydration shells surrounding peptides affect the energy landscape of self-assembly process, influencing the kinetics, conformation, surface binding, and stability of different peptide assembly configurations, and provide dynamic flexibility, [17] which, in turn, affect their ability to self-assemble into ordered nanostructures on solid surfaces. While the effect of solvents is acknowledged, [18] no experimental results have detailed peptide hydration structures in 3D interfacial space with sub-nanometer spatial resolution. The hydration of a protein influences binding and selectivity, affecting the reactivity and interaction with other molecules, which are crucial for their applications in sensing, linking and catalysis.<sup>[19,20]</sup> This effect arises mainly from the additional energetic penalty imposed by the hydration shells during ion interactions with the peptide surface in host-guest binding, as the structured water layers must be displaced to enable the peptide and host to make close direct contact.[21]

The first limitation is largely overcome by the use of self-assembling solid-binding peptides, as demonstrated in numerous studies that show the controlled organization of 10–15 amino acid long wild-type or mutant peptides with predictable structures and electronic properties.<sup>[7,12–14,22–29]</sup> For the second constraint, the atomic force microscopy (AFM) emerges as a standout technique that provides sub-nanometer structural details of complex biomolecular structures under aqueous environments.<sup>[12,14,30–34]</sup> The third challenge—understanding the role of water or solvent in the assembly process—can be tackled using an advanced 3D-AFM measurement technique based on small-amplitude oscillations,<sup>[31,35]</sup> which provides unprecedented structural resolutions<sup>[32,36–39]</sup> for determining the molecular arrangements of the 3D local hydration/solvation structures.

Here, we examined a simple dipeptide known to self-organize on atomically flat solid interfaces, such as graphite and MoS<sub>2</sub>.<sup>[27]</sup> We chose tandem repeats of a dipeptide with amino acids having aromatic side groups, tyrosine (Y) and histidine (H) with phenol and imidazole side chains, respectively. We investigated the assembly behavior of nr-YH peptides, where n is the number of repeating (YH) units. We analyzed the 2D assemblies on surfaces by AFM, while the 3D structures in solution were studied with circular dichroism (CD) spectroscopy; the secondary structures of the peptides on graphite in water were assessed using ATR-FTIR spectroscopy, and molecular modeling based on density-functional theory (DFT), neural network potentials (NNP), and

M. Sarikaya DMXi Dentomimetix, Inc. 3729 NE 194th Str., Seattle, WA 98155, USA

### 2. Results and Discussion

# 2.1. Molecular Organization of nr-YH Peptide Assemblies on Graphite and ${\rm MoS}_2$

flexible transistors, sensors, and memory devices.[40]

The nr-YH peptides shown in Figure 1A are short amphiphilic dipeptides composed of alternating amino acid sequences: tyrosine, which is non-polar and hydrophobic, and histidine, which is polar, hydrophilic, and mostly neutral at pH 7.0. This combination of sequences allows nr-YH peptides to self-assemble into various nanostructures through a balance of intermolecular interactions among peptides and the surface. Histidine is an amino acid characterized by the presence of an imidazole ring in its side chain and plays an important role as a catalytic residue in the active sites of many enzymes. [41,42] It is essential for protein functionality, particularly for proton transfer.[43] Furthermore, leveraging histidine's strong affinity for lipid membranes, several studies have been conducted to develop cell-penetrating peptides that incorporate histidine residues for the targeted delivery of biomolecules into cells.[44,45] Our results showed that peptides with n > 2 consistently form well-ordered crystalline assemblies, whereas 2r-YH tends to form aggregates, clusters, or single particles instead of stable crystalline structures (Figure 2; Figures S1 and \$2, Supporting Information). Examples of self-organized 3r-YH, 4r-YH, and 5r-YH peptide assemblies on graphite show the formation of stable, densely packed, long-range-ordered, 2D crystalline nanostructures (Figure 2A-C; Figures S3 and S4, Supporting Information). The peptide assemblies arrange into oblique lattices, with lattice parameters, a, along the transverse direction differing according to their respective lengths, while identical lattice parameters are found along the longitudinal direction, b,

www.small-journal.com

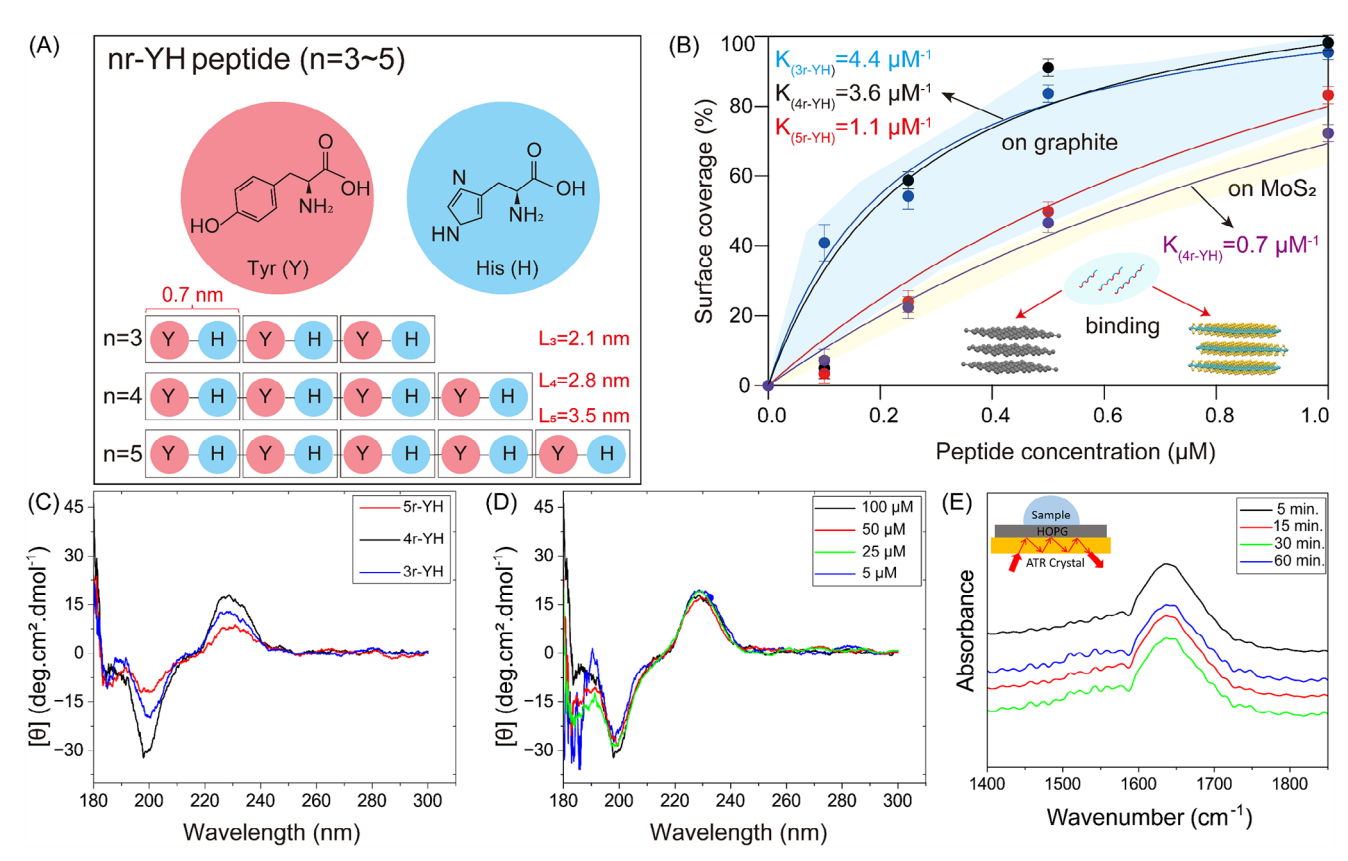


Figure 1. Molecular characteristics of nr-YH peptides (n=3,4,5). A) The molecular structure of the peptide contains two amino acids: Tyrosine, with a phenol side chain, and Histidine with imidazole ring. The schematic represents the sequences of the peptides and their lengths in their unfolded conformations. B) Binding constants of the 3r-, 4r- and 5r-YH peptide assemblies on graphite, and for the 4r-YH on MoS<sub>2</sub>. C) CD spectra of peptides in water at 100  $\mu$ M concentration. D) Concentration dependence of CD spectra for the 4r-YH peptide at 5, 25, 50, and 100  $\mu$ M. E) In situ (ATR)-FTIR spectra recorded for the 4r-YH peptide assembly on graphite at 10  $\mu$ M.

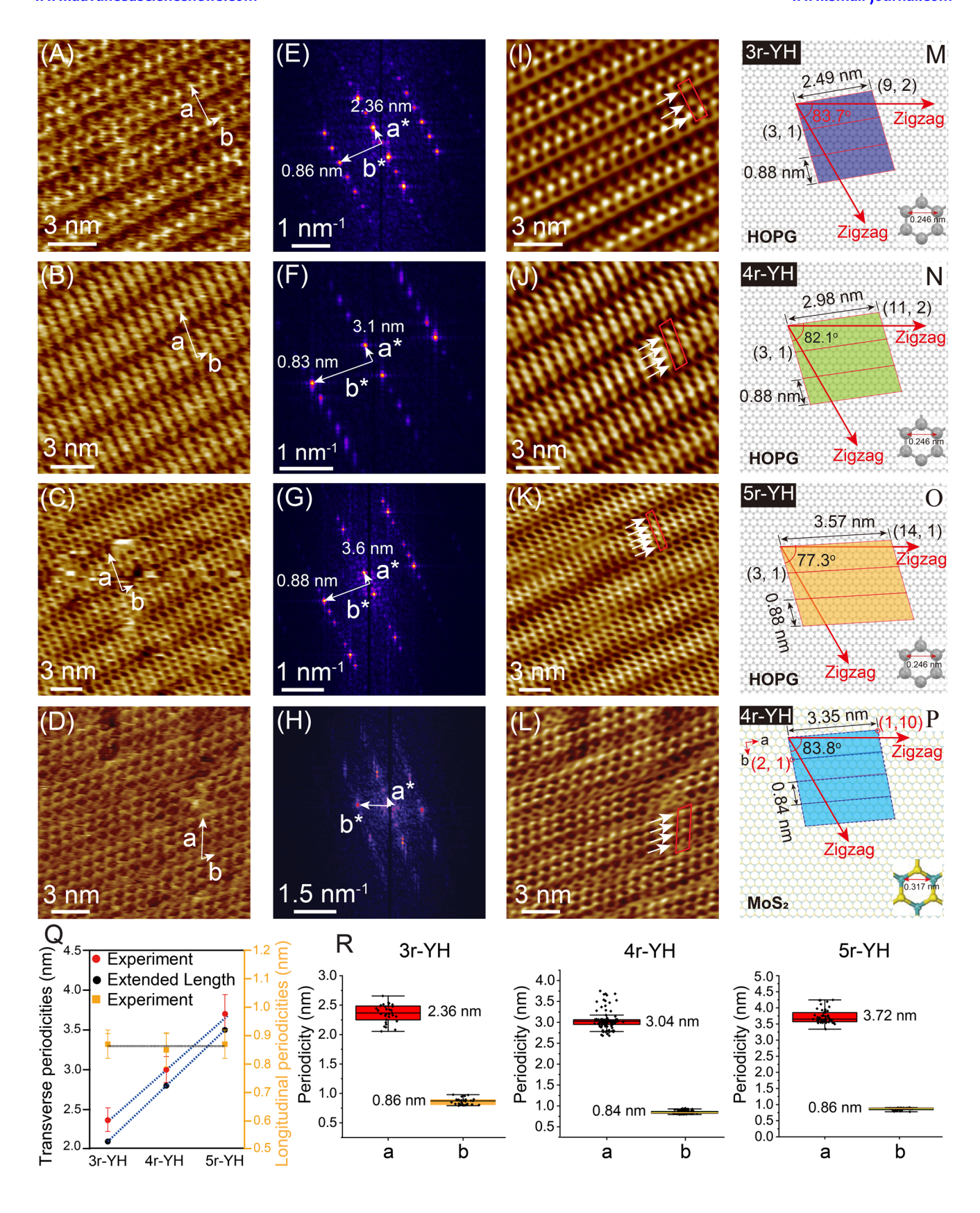
corresponding to the linear width of the peptides (Figure 2Q,R). Each peptide assembly establishes an exclusive chiral crystallographic relationship with the underlying solid atomic lattice (Figure 2M–P; Figure S5, Supporting Information). This observation suggests that solid substrate facilitates templating of the peptide for binding and assembly.

There is a strong correlation between the number of (YH) units in the peptide chain and the number of intervals between repeating molecular features in the transverse direction in the AFM images (Figure 2; Figures S3 and S4, Supporting Information). This observation suggests that the peptide chains adopt a minimally folded, linearly extended conformation within the assembled structures, as supported through the height profiles and FFT analysis (Figure 2E–G). While the values of b in all cases are 0.85  $\pm$  0.05 nm, the widths of the unit cell in the transverse direction, the values of lattice parameter a, were  $\approx 2.36 \pm 0.15$  nm for 3r-YH,  $3.04 \pm 0.21$  nm for 4r-YH, and  $3.72 \pm 0.21$  nm for 5r-YH peptide assemblies (Figure 2Q,R), with the difference in the values of a being about 0.68 nm for the successive 3r-, 4r-, and 5r-YH peptide assemblies. The observed difference in transverse unit cell widths (a values) corresponds closely to the variation in the number of amino acids among the peptides. On the other hand, a lattice parameter values are slightly larger than the fully extended lengths of each peptide and show some variations centered at about 0.2–0.3 nm (Figure 2Q,R), which can be attributed to the presence of water molecules within the hydration layer of each peptide molecule. The presence of water, therefore, would facilitate hydrogen bonding interactions, including those involving the peptide terminal groups and water molecules. These weak interactions serve as flexible bridges between peptides and facilitate subtle structural adjustments necessary during the self-organization processes. To determine the influence of the surface on the observed assembly properties, we also studied the behavior of 4r-YH peptides on  $MoS_2$  in water. The peptides also self-assemble into a long-range, ordered crystalline nanostructures on  $MoS_2$  (Figure 2D). Again, the assembled molecular lattice exhibits a four-interval lattice pattern, indicative of the peptide adopting an extended linear conformation within an oblique lattice (Figure S6, Supporting Information).

To provide a molecular-level understanding of the observed peptide assemblies, we carried out geometry relaxations (in vacuum) of dipeptide fragments on graphene using a NequIP<sup>[46]</sup> NNP. The use of an NNP is motivated by the complexity of these on-surface assemblies, which might not be fully captured by available MD force fields.<sup>[28]</sup> The NNP was trained on DFT calculations carried out with the optB86b-vdW functional,<sup>[47]</sup> within the VASP<sup>[48]</sup> framework. Using the NNP to perform geometry relaxations, we determined YH assembly configurations that

16136829, 0, Downloaded from https://onlinelibrary.wiley.com/doi/10.1002/smll.202501785 by Aalto University, Wiley Online Library on [01/10/2025]. See the Terms and Conditions (https://onlinelibrary.wiley.com/terms

-and-conditions) on Wiley Online Library for rules of use; OA articles are governed by the applicable Creative Commons License





SMQ www.small-journal.com

binding affinities between graphene and peptides with aromatic functional groups. To confirm this, we quantified the T-shaped  $\pi$ – $\pi$  stacking interactions using the NNP. Specifically, we computed the average interaction energy between an individual Y ring (obtained by removing the rest of the peptide assembly) and the HOPG surface, which gave a  $E\pi$ – $\pi$ <sub>T</sub> = -1. 42 ± 0.05 eV. For comparison, we considered a benzene dimer with the same T-shaped arrangement, in which these interactions are on the order of 0.1 eV.<sup>[53]</sup> Our  $E\pi$ – $\pi$ <sub>T</sub> includes the entire surface, not just one ring, but the computed value highlights its significance in

stabilizing the peptide assembly. We performed CD measurements in solution to provide further insights into the secondary structures and intra- and intermolecular interactions of the dipeptides (Figure 1C). All 3-5 tandem repeat peptides displayed identical CD spectra, characterized by a positive band at 228 nm, a negative absorption band at 199 nm, and a shoulder located between 210-218 nm. The spectra suggest that the peptides adopt a random coil conformation, indicating the characteristics of intrinsically disordered proteins in aqueous environments. The presence of the shoulder and the locations of peak positions, which deviate from the typical profiles, may indicate the possibility of transient  $\pi$ – $\pi$  interactions between the aromatic residues in solution. The changes in the electronic structure of the aromatic moieties, as evidenced by the shoulder and shifts in the CD spectra, suggest that these interactions may stabilize certain local peptide folded conformations, even though they may not result in a highly stable overall peptide structure in solution. Interestingly, none of the CD spectra of the tandem (YH) peptides shows concentration dependence (Figure 1D), suggesting that these transient interactions are intramolecular within a peptide rather than intermolecular among different peptides. Furthermore, the peak intensities at 228 nm indicate that 4r-YH has the highest intensity, while 5r-YH has the lowest (Figure 1C). This suggests that 4r-YH may have an optimal length for the repeating dipeptide, promoting favorable intramolecular  $\pi$ – $\pi$  stacking interactions between aromatic residues. If so, then the aromatic moieties of tyrosine or histidine may adopt a favorable orientation and create optimal spacing between them. This process may lead to the formation of more stable and ordered local conformations in 4r-YH compared to 3r-YH and 5r-YH, which results in a more pronounced CD peak, as observed. The (ATR)-FTIR studies carried out with the 4r-YH indicate that this peptide forms  $\beta$ -sheet secondary structure on HOPG in water (see details in Methods). Taken together, these results suggest that H-bonds between the backbone carbonyl O of one peptide and the H atoms of the side chains of tyrosine or histidine residues of the neighboring peptide may contribute to the formation of  $\beta$ -sheet interactions between peptides. These interactions, in addition to the primary backbonebackbone H-bonds, help to create a stable  $\beta$ -sheet assembly

matched well with the experimentally observed patterns. The optimized structures were then solvated, as detailed in the Methods section. The (YH) dipeptide sequence can, in principle, participate in  $\pi$ – $\pi$  stacking interactions. However, these interactions are not as strong as those between purely aromatic rings, such as Y-Y pairs, due to the less extensive delocalized  $\pi$  electron system in the imidazole ring of histidine. Nevertheless, it is conceivable that the presence of OH groups in tyrosine residues can strengthen the interactions between adjacent peptides by forming H-bonds with the N atoms in the imidazole ring of histidine. A simulated assembly structure of 4r-YH on graphene (Figure 3; Figures S7-S9, Supporting Information) reveals a parallel, linear molecular arrangement of individual peptides with certain laterally staggered orientations relative to the longitudinal direction (indicated by red arrows in Figure 3A,B). The molecular organization of peptides was constructed based on arrangements where different peptide termini face each other, either C-to-N or N-to-C. The aromatic moiety of tyrosine and the histidine imidazole units are positioned on opposite sides of the dipeptide backbone and are vertically aligned with an alternating arrangement, interacting with neighboring peptide aromatic rings through a half-displaced, face-to-face  $\pi$ - $\pi$  stacking arrangement. The peptide backbone is aligned along the zigzag direction of the graphite lattice, with the tyrosine and histidine aromatic rings aligned at an angle of 60° with respect to the backbone. This molecular organization forms an oblique lattice with a = 3.1 nm and b = 0.9 nm with  $\alpha = 74^{\circ}$ , which is in excellent agreement with the lattice parameters determined from our experiments (Figure 2Q,R). The spacing of 0.7 nm (corresponding to the two amino acid units) between the periodic molecular features along the peptide orientation in our simulated structures agrees well with the observed periodicity in the close-packed molecular arrangement of dipeptide assemblies in AFM experiments (Figure 2; Figure S3, Supporting Information), providing a realistic model of peptide behavior on graphite surface.

Our simulations suggest that the linear structural assembly of nr-(YH) dipeptides is mainly driven by a combination of weak interactions, including hydrophobic interactions between the peptides and the underlying graphite lattice, hydrogen bonding between the OH groups in tyrosine and the O atoms of the neighboring dipeptide backbone, the N atoms in the imidazole ring of histidine, and  $\pi$ - $\pi$  stacking interactions between tyrosine and histidine residues. Furthermore, it appears that the face-to-edge  $\pi$ - $\pi$  stacking (T-shaped) interactions between the edges of tyrosine benzene rings and the face of the hexagonal carbon lattice in graphite further stabilize the assembled dipeptide structures. It is well established theoretically that  $\pi$ - $\pi$  interactions occur between aromatic functional groups in peptide side chains and graphene surfaces, as well as between different peptide side chains and the backbone. [49-52] These interactions result in strong

Figure 2. Structural characteristics of the self-assembled nr-YH peptide on graphite and molybdenite. A–D) FM-AFM-recorded molecular resolution images of the self-assembled 3r-, 4r-, and 5r-YH peptides forming 2D lattices on graphite in water and that of 4r-YH on  $MoS_2$ . E–H) The corresponding FFT pattern obtained from the peptide assemblies in panels (A–D). The reconstructed images in (I–L) are obtained by executing inverse 2D FFT spectra (E–H). The white arrows show bright contrast features in a given peptide lattice, the number of which is consistent with the repeating YH units for each peptide assembly. M–P) Crystallographic orientation relationships between the peptide crystals and the solid lattice obtained through matching the molecular lattice of the peptide and the atomic lattice of the solids that give chiral relationship for each peptide. Q) A comparison of the peptide lengths in assembled nanostructures with their unfolded, extended lengths. R) Histogram analyses, showing the transverse and longitudinal periodicities of the peptide assemblies. All images were recorded by in situ FM-AFM using 1.5 μM peptide solutions.



www.small-journal.com

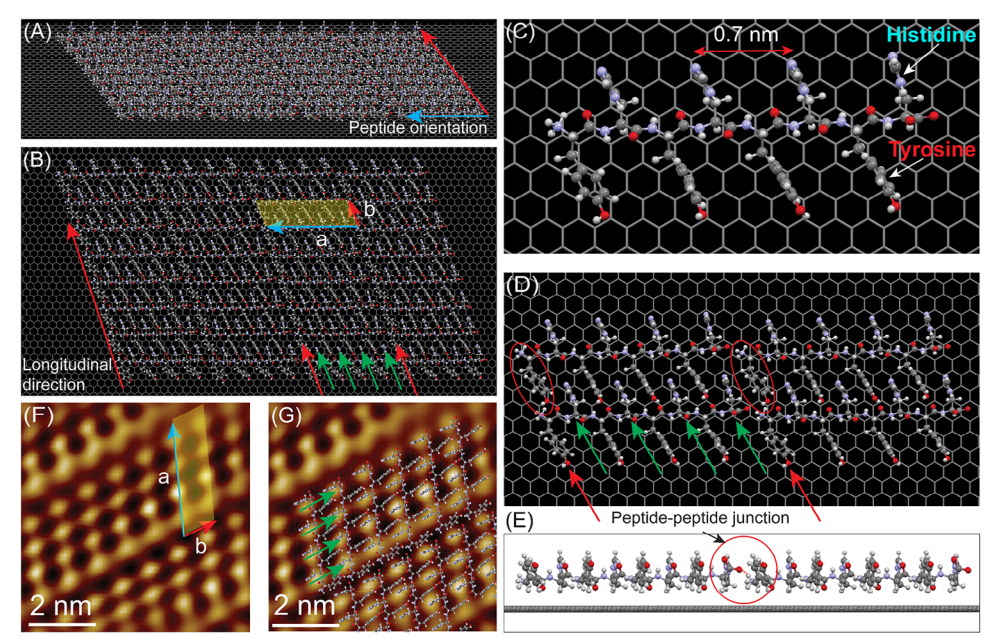


**Figure 3.** Simulated molecular arrangements of 4r-YH peptides on graphene. A,B) Oblique and top views, respectively, of the peptide assemblies showing a parallel molecular organization of individual peptides with staggered orientations. C,D) A visualization of a single and four-peptides on graphene, respectively, revealing detailed side-chain organization. The phenol of tyrosine and the imidazole of histidine are located on opposite sides of the peptide backbone and are vertically aligned, interacting through a displaced, face-to-face  $\pi$ - $\pi$  stacking interactions. The phenolic hydroxyl group (OH) of tyrosine participate in H-bonding with N of histidine and O of the adjacent peptide backbone. E) A peptide junction, showing the C- and N-terminal configurations of two peptides in the assembled structure, highlighting how the peptide end terminal moieties and the OH- group from the neighboring tyrosine can participate in H-bonding. F,G) High resolution FM-AFM images with overlaid molecular models. The green arrows indicate the four bright contrast features in the unit cell, reflecting the number of (YH) units.

reinforced by the hydrophobic interaction of tyrosine with the underlying graphite lattice.

## 2.2. 3D-AFM Measurements of Peptide-Water Interfaces

We also carried out 3D-AFM to examine the role of water in peptide assembly processes (see details in Methods). 3D-AFM is a prominent AFM technique that employs small-amplitude oscillations<sup>[35]</sup> to scan 3D interfacial surface regions and record changes in forces resulting from interactions associated with the interfacial solution or water structuring,[31-33,36,38,39,54-58] allowing the investigation of 3D molecular organizations and interactions of solvent molecules and ions within a depth of a few nanometers. Our observations revealed a highly organized arrangement of water molecules within the 3D interfacial space, reflecting the lateral periodicity and molecular symmetry of the underlying peptide assembly structure in both X and Y directions, as inferred from the vertical (Figure 4B,C) and horizontal slices (Figure 4F–M) extracted from the 3D  $\Delta f$  map in Figure 4A. This highly organized hydration layer extends ≈0.6–0.7 nm away from the nearest peptide surface into the bulk water along the z-axis. While the hydration structure exhibits a discontinuous molecular arrangement laterally near the surface (marked by green arrows in Figure 4C), following the specific chemical/structural domains of the peptide assembly, at large distances it evolves into a continuous arrangement without molecular ordering (highlighted by the red arrow in Figure 4B,C; Figures S10 and S11, Supporting Information). This featureless molecular organization at large distances is identical to the hydration layer formed on hydrophobic surfaces. [58] The 2D vertical  $\Delta f$  hydration pattern acquired along the transverse direction indicates four distinct domains (Figure 4C; marked by green arrows) indicating that the molecular structure of the hydration layer reflects the 2D structural arrangement of the 4r-YH peptide assembly, with four interval lattice patterns spaced at  $\approx$ 0.7 nm. The evaluation of the 2D XY  $\Delta f$  slices through the hydration layers indicates that the well-ordered hydration features gradually disappear, and structures become visible only along the longitudinal direction (Figure 4F–M). This structural transition from a highly ordered to a less ordered structure is evident from the decrease in the intensity of the FFT spots (Figure 4N) and the power spectral density (Figure 4O).

We performed MD simulations to gain a molecular-level understanding of the observed organization of water on peptides and its role in the formation of peptide assemblies on graphite. To do this, the structure previously optimized with the NNP in vacuum was positionally restrained, solvated with water, and then simulated using classical MD, as detailed in the Methods section. Classical MD was utilized because of the prohibitive computational cost of using NNPs in ns production runs containing tens of thousands of water molecules. At the same time, the position constraints on YH were necessary since the potential energy surfaces of the NNP and MD force field are different, and, especially for such a complex system, this difference can lead to significant structural changes. The simulated 3D distribution of wateroxygen density around peptide assemblies on bilayer graphene shows a highly organized, complex density pattern with localized

16136289, 0, Downloaded from https://onlinelibrary.wiley.com/doi/10.1002/sml1.202501785 by Aalto University, Wiley Online Library on [01/10/2025]. See the Terms and Conditions (https://onlinelibrary.wiley.com/terms-and-conditions) on Wiley Online Library for rules of use; OA articles are governed by the applicable Creative Commons Licensean

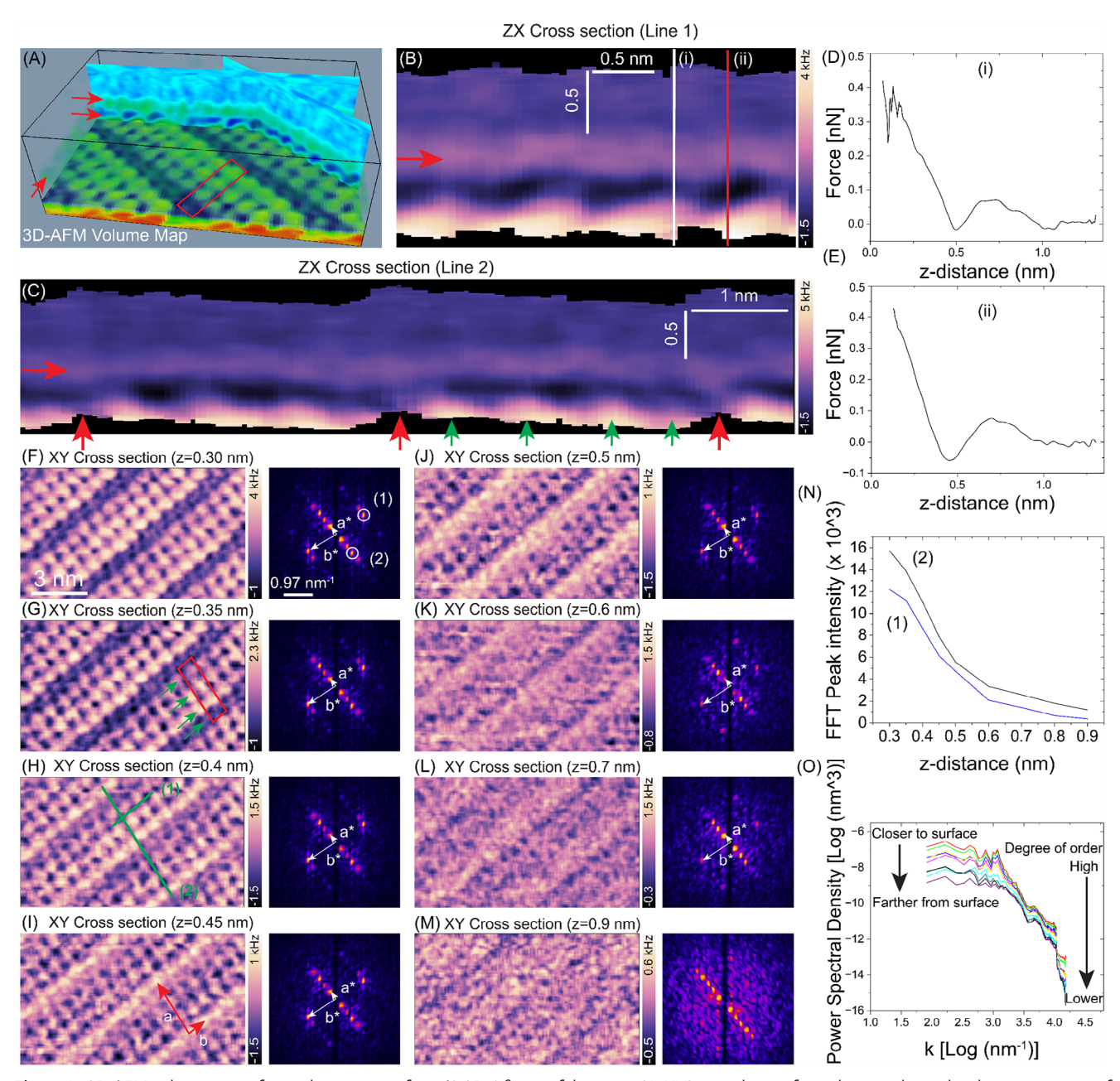


**Figure 4.** 3D-AFM volume map of peptide-water interface. A) 3D  $\Delta f$  map of the water-(4r-YH) peptide interface, showing the molecular organization of water near the assembled peptide surface in the 3D interfacial space. B,C) The ZX slices provide 2D vertical maps taken along the green lines labeled (1) and (2) in (H), respectively. It can be noticed that the hydration pattern taken along (2) indicates four domains within a unit cell (marked by green arrows), reflecting the 2D structural arrangement of the 4r-YH peptide assembly. D,E) Force-distance curve converted from  $\Delta f$  using the Sader method, acquired along the white and red lines labeled as (i) and (ii) in (B). F–M) 2D XY horizontal  $\Delta f$  slices extracted from the 3D map in (A) and their corresponding FFT patterns. The red rectangles indicate the unit cell lattice of the 2D hydration structure. N) The changes in the FFT peak intensity as a function of z-distance through hydration layers for the spots labeled (1) and (2) in (F). O) Changes in the power spectral density of FFT patterns at varying distances from the surfaces. The scale bar in (F) applies to panels (F–M).

regions of increased density extending across the entire XY plane (Figure 5A,B). The averaged vertical 1D water-oxygen density plot as a function of distance shows that this well-structured water density distribution fades away beyond  $\approx$ 0.6 nm from the surface (Figure 5C), in excellent agreement with the experiment. The 3D water oxygen density distribution was analyzed to extract a 2D

in-plane representation of the density distribution (Figure 5D–I), allowing for a direct comparison with the hydration structures obtained from experiments (Figure 4F–M). Closer to the assembly surface, the water density distribution exhibits a distinct pattern, with the high-density regions clustered around the peptide side chains possibly arising from direct H-bonding between the



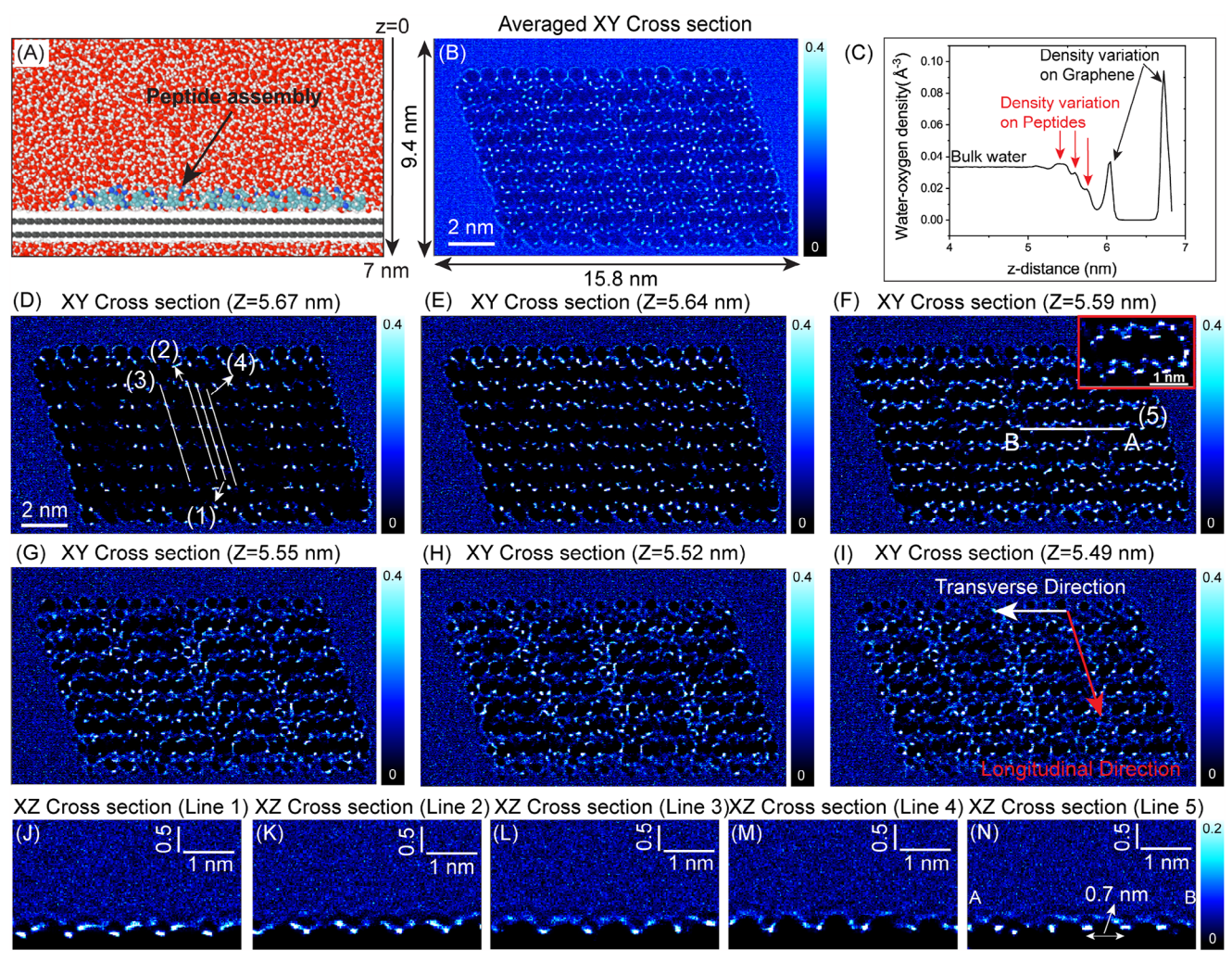


Figure 5. Simulated water-oxygen density distribution around 4r-YH peptide assemblies on bilayer graphene. A) An MD snapshot showing the peptide assemblies on a graphene bilayer in water. The water molecules are depicted in a continuous van der Waals surface. B) A 3D map of the water oxygen density distribution around the peptide nanostructures. C) A vertical 1D density-distance curve, illustrating the water density distribution both on peptide and graphene layers. D-I) 2D horizontal water density slices extracted from the 3D map at different z positions. J-M) Vertical 2D density profile of water-O atoms above the peptide nanostructure, taken along the white lines marked in panel (D). N) Vertical 2D density profile of water-O atoms above the peptide, taken along the transverse direction, marked in (F).

hydrophilic moieties of the peptide and the surrounding water molecules. As the distance from the surface increases, the welldefined bright density features evolve into a relatively darker contrast with no clear localization, indicating a change in the nature of the peptide-water interactions (Figure 5H,I). At large distances, the high-water density is mainly located along the longitudinal direction at the interface where two peptides join (red arrow in Figure 5I). This organization at the interface may be attributed to the specific arrangement of tyrosine residues within the peptide assembly. Due to the relatively tilted orientation of these residues—rather than being perfectly vertically aligned like those at the center, as determined by calculating the angle and center-of-mass distance between each tyrosine benzene ring and its adjacent graphite hexagonal ring<sup>[59]</sup> (see Figures S12 and S13, Supporting Information)—hydrophobic domains are exposed to water along the longitudinal direction. This exposure results in the expulsion of water molecules from the immediate surface

regions, leading to the confinement of water at larger distances from the peptide surface.

The 2D in-plane density distribution and snapshots with overlaid molecular structure reveal four bright features of high-water density regions (**Figure 6B**,C), extracted from the 3D density map (Figure 6A). These features closely align with the experimentally obtained 2D horizontal XY  $\Delta f$  patterns, where three prominent and one faint hydration features appear within the unit cell (Figure 6D) with identical periodicities of 0.7 nm along the transverse direction. This observation demonstrates that water structuring follows the four domains of underlying peptide assemblies in the unit cells. The displaced face-to-face molecular arrangement of the histidine and tyrosine aromatic moieties attracts water molecules to these regions, resulting in a higher local density of water. This particular geometric arrangement may also confine water molecules around these areas, similar to the stabilizing role of directional H-bonds in protein structures. In



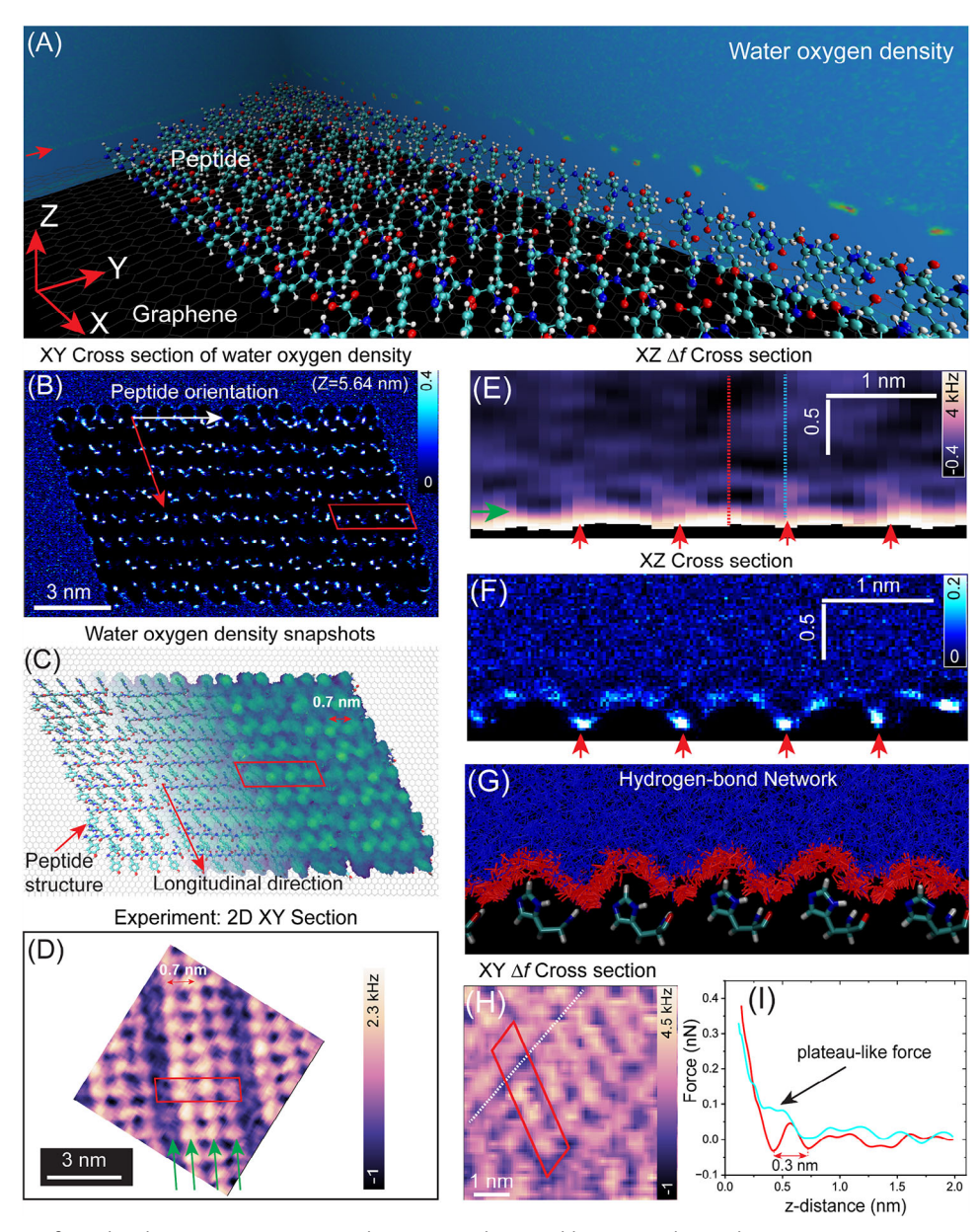


Figure 6. Comparison of simulated water structuring around 4r-YH peptide assemblies on graphite with experiments. A) 3D water density distribution with overlaid peptide assembly structures on graphene, showing 2D vertical ZX/ZY slices. B) 2D XY water oxygen density distribution at z = 5.64 nm, revealing the variation in water density across the peptide assemblies. C) 100 snapshots of water oxygen density distribution with the underlying peptide self-assembled structures are overlaid. D) 2D XY  $\Delta f$  slices extracted from the 3D map. The red rectangle indicates the unit cells of 2D hydration structure. E) 2D vertical XZ Δf slice taken along the dashed line in (H). F) 2D vertical density profile of water oxygen atoms above the peptide nanostructures, taken along the longitudinal direction. G) Corresponding water hydrogen network formed. H) 2D XY  $\Delta f$  slice extracted from the 3D map. I) Force-distance curve derived from the Δf based on Sader method, acquired along the red and cyan dashed lines in (E). The red arrows in (E) and (F) indicate the identical locations.

contrast, at the joint where two peptides merge in a head-to-tail manner, the hydrophobic pore of the tyrosine ring is exposed to water, leading to a relatively less localized water density, similar to that on a hydrophobic surface. The 2D density snapshots reveal that water primarily interacts with the OH groups in the tyrosine residues and the N atoms in the imidazole ring of histidine, leading to the confinement of water around these regions. The simulated water oxygen density distribution also replicates most of the experimentally observed hydration features in the 2D vertical XZ  $\Delta f$  map along the longitudinal direction. The 2D vertical XZ  $\Delta f$  map taken along the longitudinal direction (Figure 6E) exhibits an undulating hydration feature with a periodicity of 0.85 nm, consistent with the simulated water-O density distribution (Figure 6F). The 2D density snapshots and corresponding H bonding networks, superimposed on the molecular structures of the peptide assembly, reveal a preferential interaction between



water molecules and the O atoms of the peptide backbone, as well as with the H and N atoms of the histidine residues. This interaction results in a closer proximity of water molecules to the surface above the backbone O atoms, while positioning them at relatively higher levels above the histidine residues, creating an intricate arrangement that gives rise to an undulating water density profile (Figure 6F,G; Figures S14 and S15, Supporting Information), in agreement with the experiments.

The hydration force can be quantified by converting  $\Delta f$  measurements into force using the Sader method to understand the nature of interactions between water and peptides. Here, two distinct types of force curves were observed – one displaying a clear oscillatory profile, corresponding to the hydration forces, and the other exhibiting a plateau-like force curve (Figure 6I). The latter is a characteristic of the interactions of water strongly bound to the surface functional groups, likely through H-bonding. The H-bond analyses (Figure \$16, Supporting Information) show a significant number bonds forming between water molecules and the peptide C-terminal oxygen (labeled OG2D2), the hydrogen atoms in the NH and OH groups of histidine and tyrosine (labeled HGP1), and the backbone hydrogen atoms, as well as between the nitrogen atoms of histidine (labeled NG2R50). Additionally, a significant number of HBs form between water molecules and the peptide backbone oxygen atoms (labeled OG2D1). The observed close correlation highlights the strong relationship between the peptide assembly structure and the specific arrangement of water in the hydration layer, suggesting that water may play a crucial role in mediating interpeptide molecular interactions, stabilizing specific conformations, and facilitating assembly.

### 3. Conclusion

Here, we show that simple dipeptides with nr-YH tandem repeats can be designed to self-organize into long-range ordered assemblies, forming molecular-thick 2D crystalline lattices on atomically flat inorganic surfaces with hexagonal symmetry, such as graphite and MoS<sub>2</sub>. The exclusive lattice formed by each of the tandem peptides has a lattice parameter equivalent to the linear, unfolded length of the peptide, suggesting that there is a strong interaction between the aromatic moieties of the amino acids and the hexagonal organization of carbon atoms in graphite and those of sulfur in MoS<sub>2</sub>. The interplay between aromatic interactions and solvation effects significantly influences the self-assembly of dipeptides on solid surfaces. Water plays a critical role by facilitating intermolecular interactions through H-bonding, thereby enabling conformational flexibility during the self-assembly process on substrates. Furthermore, the peptide-water interactions and resulting water structuring that encapsulates the peptide surfaces are crucial for providing flexibility and selectivity to the peptide chains, allowing them to adapt and respond to environmental changes. The heterogeneity in the extent and structure of hydration shells on the peptide surface suggests the presence of specific binding pockets that could play a crucial role in mediating selective interactions with other biomolecules. Understanding water-peptide interactions through 3D-AFM measurements helps in the design and engineering of peptide sequences with specific properties and is important for understanding various phenomena such as protein folding, stability, and molecular recognition. These well-organized, closely packed, long-range ordered peptide assemblies could serve as templates for the 1 or 2D directed organization of inorganic nanoparticles, [60] allowing control over interparticle distances at sub-nanometer resolution and enabling the study of their quantum mechanical properties. The YH peptide can act as a building block for the design of catalysts that mimic the active sites of natural enzymes by forming catalytically active pockets through the spatial arrangement of the peptide side groups. Additionally, these stable assemblies support biomolecule immobilization, providing platforms for studying molecular recognition and enabling the development of high-performance catalytic interfaces for electrochemical applications.<sup>[61]</sup> Overall, this study provides a novel perspective on the role of water in mediating peptide self-assembly, highlighting the importance of specific peptide sequences for generating well-defined, functional nanostructures. We emphasize that the properties of the solvent, particularly its polarity and hydrogen bonding capabilities, play a critical role in determining the structural organization, assembly mechanisms, and interfacial structures of peptide assemblies, highlighting a promising direction for future research. Our ongoing research aims to unravel the local hydration structures surrounding solid-binding peptides, providing deeper insights into how hydrophobic and hydrophilic amino acid sequences influence the interfacial molecular organization of water within the hydration zone, toward a better understanding of the molecular mechanisms of commensurate peptide assemblies on solid surfaces.

## 4. Experimental Section

*Peptide Solution*: 19.2 mg of 3r-YH, 29 mg of 4r-YH, and 19.8 mg of 5r-YH, peptide powders (purities > 98%, as verified high performance liquid chromatography measurements) were provided by GL Biochem (Shanghai) Ltd. Their molecular weights are 918.95, 1219.26, and 1519.57 g mol $^{-1}$ , as confirmed by Mass spectrum measurements, respectively. Prior to the AFM measurements, the peptide powders were dissolved in ultrapure water to obtain peptide solutions with a concentration of 100 μM for 3r-YH, 4r-YH, and 5r-YH. The prepared peptide solutions were stored in -20 °C refrigerator. Depending on the experimental needs, the stock solution was diluted into different concentrations of 0.1–10 μM.

Sample Preparation for AFM Observations: As substrates for peptide self-assembly, freshly exfoliated highly oriented pyrolytic graphite (HOPG; grade ZYA, mosaic spread  $0.4\pm0.1^{\circ}$ ) and single-crystal, highly oriented synthetic 2H-phase molybdenum disulfide (MoS $_2$ ; mosaic spread  $0.3^{\circ}$ , purchased from 2D Semiconductors) crystals were used. Prior to incubation on the substrates, stock solutions of 3r-YH, 4r-YH, and 5r-YH peptides were equilibrated to room temperature. Subsequently, 120  $\mu L$  of each peptide solution was immediately deposited onto the graphite and MoS $_2$  surfaces and allowed to incubate for 10 min at room temperature. Following incubation, the samples were rinsed 2–3 times with water and subjected to FM-AFM investigation to characterize the molecular structures of the self-assembled peptides under liquid conditions.

FM-AFM Setup: The surface and interface structural characterization of self-assembled nr-YH peptides on HOPG and  ${\rm MoS}_2$  were realized with a homemade FM-AFM system operating in liquid environments equipped with an ultra-low noise cantilever deflection sensor. [62] The oscillation of the AFM cantilever was driven by photothermal excitation with an infrared laser beam with a wavelength of 785 nm. The homemade AFM scanning was controlled by a commercial AFM controller (ARC2, Asylum Research), and the amplitude of cantilever oscillation was kept constant using a commercially available controller (OC4, SPECS). The AFM was operated in constant frequency shift ( $\Delta f$ ) mode, where the tip-sample distance is adjusted such that  $\Delta f$  is kept constant. The AFM images were acquired with





www.small-journal.com

160AC-NG cantilevers (purchased from OPUS) with a nominal spring constant of 26 N m $^{-1}$  and a nominal tip radius <8 nm. This work also used AC55 cantilevers (from Olympus) with a nominal spring constant of 85 N m $^{-1}$  and a nominal tip radius <8 nm, with a resonance frequency of 1.6 MHz. The individual spring constant of each cantilever was experimentally determined using the standard thermal tune method,  $^{[63]}$  after each experiment. The scan rates and scan angle were adjusted to obtain a better resolution of the surface features. AFM image rendering and data processing were performed by using the WSxM and Gwyddion image analysis software. No filter was applied during the AFM scanning process.

3D-AFM Measurements: The analysis of the 3D local hydration structures surrounding self-assembled YH peptide structures on graphite in water was carried out using 3D-AFM force mapping experiments. The 3Dfrequency shift ( $\Delta f$ ) maps of the interfaces between the peptide and water were generated employing the previously established 3D force mapping methodology as described in Refs.[32,37] In particular, an additional fast sinusoidal modulation was simultaneously implemented on the z-piezo movement to precisely control the vertical position of the tip during image acquisition and force mapping. This z-piezo signal was synchronized with the lateral xy scanning movements of the tip, allowing for the recording of  $\Delta f$  at each tip location while maintaining a constant average distance between the tip and the sample to ensure a stable  $\Delta f$  set-point. Consequently, this technique helped to produce a detailed map in which each pixel within the 3D interfacial space is associated with a distinct  $\Delta f$  value. As the tip approached the surface, an oscillatory force acted upon it as a result of the displacement of the structured water layer at these interfaces. A 3D- $\Delta f$  map covering an area of  $\approx$  (15–20)  $\times$  (15–20) nm was acquired through real-time recording of  $\Delta f$  relative to the tip positions in the 3D interfacial space between the peptide nanostructures and the surrounding water. The typical resolution of the 3D  $\Delta f$  datasets was set at 128  $\times$  128 pixels in the lateral dimensions and 256 pixels in the vertical dimension, prior to any data interpolation applied in certain instances. The cantilever oscillation amplitudes were adjusted within a range of 0.1 to 0.25 nm, which is less than the size of a water molecule, thereby helping to clearly distinguish the distribution of local hydration layers. The modulation signal in the z-direction during the 3D-AFM force mapping was characterized by a frequency of 195.3 Hz and an amplitude in the range of 2–3 nm. The results obtained from the 3D AFM were presented in terms of the  $\Delta f$  corresponding to the interaction between the tip and the sample. The resultant 3D- $\Delta f$ map was subsequently transformed into a 3D force map utilizing Sader's method.

Circular Dichroism Measurements: To investigate the secondary structure formation in solution, CD spectroscopy measurements were performed using a Jasco J-1500 spectrophotometer (JASCO Corporation, Tokyo, Japan). All CD measurements were conducted in a cuvette with an optical path length of 0.5 mm at room temperature (25 °C) in the wavelength range of 180 to 300 nm. Each CD spectrum was averaged from three scans, and the corresponding water baseline was subtracted from the sample spectrum to correct for background scattering.

Attenuated Total Reflectance-Fourier Transform Infrared Spectroscopy Measurements: (ATR)-FTIR measurements were performed at room temperature using a JASCO Fourier Transform IR-4700 spectrophotometer in the range between 7800 and 350 cm $^{-1}$ . The (ATR)-FTIR spectra for different incubation times of peptides were recorded for 5, 10, 15, 20, 30, and 60 min. The spectrometer involves a diamond crystal internal reflective prism. The sample solution (10  $\mu$ M of 4r-YH peptide solution) was incubated on the diamond crystal cell, and then a freshly prepared HOPG substrate was brought into mechanical contact with the underlying sample solution by inverting the surface. The amide I band was observed at different incubation times on the graphite substrate with peak positions in the range of 1637–1641 cm $^{-1}$ . This clearly indicates that 4r-YH peptides form  $\beta$ -sheet secondary structures on HOPG in water.

Computational Details: An individual 3r-, and 4r-YH peptide was constructed with NH $_3$ <sup>+</sup> as the N-terminus and COO- as the C-terminus. Following an initial arrangement inferred from the experimental data, a 2  $\times$  2 3r-YH and 4r-YH supercell was assembled, placed on a graphite substrate and the geometry was relaxed. This relaxation was done using a NequIP<sup>[46]</sup> NNP. The NNP was trained on a dataset of DFT calculations of peptide

fragments on HOPG, calculated using the optB86b-vdW functional<sup>[47]</sup> in VASP. [48] The NNP had a cutoff radius of r = 7.5 Å, and its final validation errors were of a force Mean Absolute Error (MAE) of 48.9 meV Å-1 and an energy MAE of 0.956 meV atom<sup>-1</sup>. In geometry relaxation, the NNP was used as an ASE<sup>[64]</sup> calculator, together with a BFGS optimizer and a stopping force threshold of 0.05 eV  $Å^{-1}$ . In the final structure, the tyrosine and histidine rings were arranged vertically in an alternating pattern. The  $2 \times 2$  supercell was then replicated into a  $4 \times 8$  one, which was then solvated, giving a total of 101 867 atoms. Since the system was neutral, no ions were added. Subsequently, the simulation of water density was carried out. First, this density was simulated in Gromacs, using CHARMM36<sup>[65]</sup> and TIP3P, and letting only the water molecules move freely by setting position restraints on 4r-YH and HOPG. After carrying out a 5 ns equilibration, a 10 ns NVT production run was used to extract the water oxygen density using MDAnalysis.<sup>[66]</sup> The system was first equilibrated in NVT for 5 ns at T = 298 K, using the V-rescale thermostat with a time constant of  $\tau = 0.1$  ps. A 1 fs timestep was utilized. Electrostatics were computed using PME with a 1.2 nm cutoff and 0.125 nm grid spacing, and van der Waals interactions employed a cutoff of 1.2 nm with force-switching from 1.0 nm. Then, a 10 ns production run was carried out using the same settings but with  $\tau = 1.0$  ps. Finally, the water oxygen density was extracted using MDAnalysis. A 0.1 Å grid was utilized, and frames were sampled at 10 ps intervals.

## **Supporting Information**

Supporting Information is available from the Wiley Online Library or from the author.

## **Acknowledgements**

This work was primarily supported by Grants-in-Aid for Scientific Research (21H05251, 24K01316, 24H01124, 22H05408, and 20H02564) from the Ministry of Education, Culture, Sports, Science, and Technology of Japan (MEXT) and Research Council of Finland (project no. 347319). This work was also partially supported by the World Premier International Research Center Initiative (WPI), MEXT, Japan, and by JST CREST (Grant number JPMJCR24A4). The computing resources from the Aalto Science-IT project, CSC, and Helsinki are gratefully acknowledged.

#### **Conflict of Interest**

The authors declare no conflict of interest.

## **Author Contributions**

A.Y. performed AFM experiments, conducted data analyses, and prepared the first draft of the manuscript with M.S., F.P. performed the simulations. L.S. contributed to the peptide preparation and data analyses. Y.H. assisted with peptide preparation while M.S. provided guidance in molecular assembly. S.K. and K.M. performed CD and (ATR)-FTIR measurements. K.M. and K.M. developed software for 3D-AFM analyses. A.Y. and T.F. supervised the work. A.S.F. supervised the simulations. All authors contributed to the revision and preparation of the manuscript.

### **Data Availability Statement**

The data that support the findings of this study are available from the corresponding author upon reasonable request.

## Keywords

atomic force microscopy, graphite, MD simulations, molecular self-assembly, molybdenite, peptide hydration, YH dipeptide



Received: February 11, 2025 Revised: May 27, 2025 Published online:

- A. Levin, T. A. Hakala, L. Schnaider, G. J. L. Bernardes, E. Gazit, T. P. J. Knowles, Nat. Rev. Chem. 2020, 4, 615.
- [2] M. Sarikaya, C. Tamerler, A. K. Y. Jen, K. Schulten, F. Baneyx, Nat. Mater. 2003, 2, 577.
- [3] E. Gazit, Chem. Soc. Rev. 2007, 36, 1263.
- [4] Y. Yamazaki, T. Hitomi, C. Homma, T. Rungreungthanapol, M. Tanaka, K. Yamada, H. Hamasaki, Y. Sugizaki, A. Isobayashi, H. Tomizawa, M. Okochi, Y. Hayamizu, ACS Appl. Mater. Interfaces 2024, 16, 18564.
- [5] H. Noguchi, Y. Nakamura, S. Tezuka, T. Seki, K. Yatsu, T. Narimatsu, Y. Nakata, Y. Hayamizu, ACS Appl. Mater. Interfaces 2023, 15, 14058.
- [6] D. Khatayevich, T. Page, C. Gresswell, Y. Hayamizu, W. Grady, M. Sarikaya, Small 2014, 10, 1505.
- [7] J. Chen, E. Zhu, J. Liu, S. Zhang, Z. Lin, X. Duan, H. Heinz, Y. Huang, J. J. De Yoreo, *Science* **2018**, *362*, 1135.
- [8] Y. Hayamizu, C. R. So, S. Dag, T. S. Page, D. Starkebaum, M. Sarikaya, Sci. Rep. 2016, 6, 33778.
- [9] C. Homma, M. Tsukiiwa, H. Noguchi, M. Tanaka, M. Okochi, H. Tomizawa, Y. Sugizaki, A. Isobayashi, Y. Hayamizu, Biosens. Bioelectron. 2023, 224, 115047.
- [10] A. A. Mohamed, H. Noguchi, M. Tsukiiwa, C. Chen, R. S. Heath, M. Q. E. Mubarak, T. Komikawa, M. Tanaka, M. Okochi, S. P. de Visser, Y. Hayamizu, C. F. Blanford, Adv. Funct. Mater. 2022, 32, 2207669.
- [11] O. Nakano-Baker, H. Fong, S. Shukla, R. V. Lee, L. Cai, D. Godin, T. Hennig, S. Rath, I. Novosselov, S. Dogan, M. Sarikaya, J. D. MacKenzie, Biosens. Bioelectron. 2023, 229, 115237.
- [12] A. Yurtsever, L. Sun, K. Hirata, T. Fukuma, S. Rath, H. Zareie, S. Watanabe, M. Sarikaya, ACS Nano 2023, 17, 7311.
- [13] C. Chen, A. Yurtsever, P. Li, L. Sun, ACS Appl. Mater. Interfaces 2024, 16, 19699.
- [14] A. Yurtsever, K. Hirata, R. Kojima, K. Miyazawa, K. Miyata, S. Kesornsit, H. Zareie, L. Sun, K. Maeda, M. Sarikaya, T. Fukuma, Small 2024, 20, 2400653.
- [15] J. Lee, M. Ju, O. H. Cho, Y. Kim, K. T. Nam, Adv. Sci. 2019, 6, 1801255.
- [16] G. Wei, Z. Su, N. P. Reynolds, P. Arosio, I. W. Hamley, E. Gazit, R. Mezzenga, Chem. Soc. Rev. 2017, 46, 4661.
- [17] M.-C. Bellissent-Funel, A. Hassanali, M. Havenith, R. Henchman, P. Pohl, F. Sterpone, D. van der Spoel, Y. Xu, A. E. Garcia, *Chem. Rev.* 2016, 116, 7673.
- [18] S. Zhang, J. Chen, J. Liu, H. Pyles, D. Baker, C.-L. Chen, J. J. De Yoreo, Adv. Mater. 2021, 33, 1905784.
- [19] J. A. Rupley, G. Careri, in Advances in Protein Chemistry, Vol. 41 (Eds.: C. B. Anfinsen, F. M. Richards, J. T. Edsall, D. S. Eisenberg), Academic Press, Boca Raton, 1991, p. 37.
- [20] G. Otting, E. Liepinsh, K. Wüthrich, Science 1991, 254, 974.
- [21] D. T. Gomez, L. R. Pratt, D. N. Asthagiri, S. B. Rempe, Acc. Chem. Res. 2022, 55, 2201.
- [22] C. R. So, Y. Hayamizu, H. Yazici, C. Gresswell, D. Khatayevich, C. Tamerler, M. Sarikaya, ACS Nano 2012, 6, 1648.
- [23] C. Tamerler, M. Duman, E. E. Oren, M. Gungormus, X. Xiong, T. Kacar, B. A. Parviz, M. Sarikaya, Small 2006, 2, 1372.
- [24] C. R. So, C. Tamerler, M. Sarikaya, Angew. Chem., Int. Ed. 2009, 48, 5174.
- [25] M. Xiao, S. Wei, Y. Li, J. Jasensky, J. Chen, C. L. Brooks, Z. Chen, Chem. Sci. 2018, 9, 1769.
- [26] T. R. Walsh, M. R. Knecht, Chem. Rev. 2017, 117, 12641.
- [27] W. Luo, C. Homma, Y. Hayamizu, Langmuir 2023, 39, 7057.
- [28] Z. E. Hughes, T. R. Walsh, Nanoscale 2018, 10, 302.

- [29] L. Sun, P. Li, T. Seki, S. Tsuchiya, K. Yatsu, T. Narimatsu, M. Sarikaya, Y. Hayamizu, Langmuir 2021, 37, 8696.
- [30] H. Asakawa, K. Ikegami, M. Setou, N. Watanabe, M. Tsukada, T. Fukuma, *Biophys. J.* 2011, 101, 1270.
- [31] T. Fukuma, R. Garcia, ACS Nano 2018, 12, 11785.
- [32] A. Yurtsever, P.-X. Wang, F. Priante, Y. Morais Jaques, K. Miyazawa, M. J. MacLachlan, A. S. Foster, T. Fukuma, Sci. Adv. 2022, 8, abq0160.
- [33] C. Garcia-Sacristan, V. G. Gisbert, K. Klein, A. Šarić, R. Garcia, ACS Nano 2024, 18, 18485.
- [34] A. Yurtsever, H. Asakawa, Y. Katagiri, K. Takao, K. Ikegami, M. Tsukada, M. Setou, T. Fukuma, Nano Lett. 2025, 25, 98.
- [35] F. J. Giessibl, Rev. Mod. Phys. 2003, 75, 949.
- [36] A. Yurtsever, P.-X. Wang, F. Priante, Y. M. Jaques, K. Miyata, M. J. MacLachlan, A. S. Foster, T. Fukuma, Small Methods 2022, 6, 2200320.
- [37] S. Nagai, S. Urata, K. Suga, T. Fukuma, Y. Hayashi, K. Miyazawa, Nanoscale 2023, 15, 13262.
- [38] K. Miyata, J. Tracey, K. Miyazawa, V. Haapasilta, P. Spijker, Y. Kawagoe, A. S. Foster, K. Tsukamoto, T. Fukuma, *Nano Lett.* 2017, 17, 4083.
- [39] E. Nakouzi, A. G. Stack, S. Kerisit, B. A. Legg, C. J. Mundy, G. K. Schenter, J. Chun, J. J. De Yoreo, J. Phys. Chem. C 2021, 125, 1282.
- [40] A. V. Kolobov, J. Tominaga, in Two-Dimensional Transition-Metal Dichalcogenides, Vol. 239, Springer, Berlin, 2016.
- [41] C. Zhang, R. Shafi, A. Lampel, D. MacPherson, C. G. Pappas, V. Narang, T. Wang, C. Maldarelli, R. V. Ulijn, Angew. Chem., Int. Ed. 2017, 56, 14511.
- [42] C. M. Rufo, Y. S. Moroz, O. V. Moroz, J. Stöhr, T. A. Smith, X. Hu, W. F. DeGrado, I. V. Korendovych, Nat. Chem. 2014, 6, 303.
- [43] S. Li, M. Hong, J. Am. Chem. Soc. 2011, 133, 1534.
- [44] S. Hyun, Y. Choi, H. N. Lee, C. Lee, D. Oh, D.-K. Lee, C. Lee, Y. Lee, J. Yu, Chem. Sci. 2018, 9, 3820.
- [45] Z. S. Al-Garawi, B. A. McIntosh, D. Neill-Hall, A. A. Hatimy, S. M. Sweet, M. C. Bagley, L. C. Serpell, *Nanoscale* 2017, 9, 10773.
- [46] S. Batzner, A. Musaelian, L. Sun, M. Geiger, J. P. Mailoa, M. Kornbluth, N. Molinari, T. E. Smidt, B. Kozinsky, *Nat. Commun.* 2022, 13, 2453.
- [47] J. Klimeš, D. R. Bowler, A. Michaelides, Phys. Rev. B 2011, 83, 195131.
- [48] G. Kresse, J. Hafner, Phys. Rev. B 1993, 47, 558.
- [49] S. K. Burley, G. A. Petsko, Science 1985, 229, 23.
- [50] X. Zou, S. Wei, J. Jasensky, M. Xiao, Q. Wang, C. L. Brooks III, Z. Chen, J. Am. Chem. Soc. 2017, 139, 1928.
- [51] G. Zuo, S.-g. Kang, P. Xiu, Y. Zhao, R. Zhou, Small 2013, 9, 1546.
- [52] Y. Chong, C. Ge, Z. Yang, J. A. Garate, Z. Gu, J. K. Weber, J. Liu, R. Zhou, ACS Nano 2015, 9, 5713.
- [53] M. O. Sinnokrot, E. F. Valeev, C. D. Sherrill, J. Am. Chem. Soc. 2002, 124, 10887.
- [54] D. Martin-Jimenez, E. Chacon, P. Tarazona, R. Garcia, Nat. Commun. 2016, 7, 12164.
- [55] T. Fukuma, Y. Ueda, S. Yoshioka, H. Asakawa, Phys. Rev. Lett. 2010, 104, 016101.
- [56] E. Nakouzi, S. Kerisit, B. A. Legg, S. Yadav, D. Li, A. G. Stack, C. J. Mundy, J. Chun, G. K. Schenter, J. J. De Yoreo, J. Phys. Chem. C 2023, 127, 2741.
- [57] K. Umeda, L. Zivanovic, K. Kobayashi, J. Ritala, H. Kominami, P. Spijker, A. S. Foster, H. Yamada, Nat. Commun. 2017, 8, 2111.
- [58] M. R. Uhlig, D. Martin-Jimenez, R. Garcia, Nat. Commun. 2019, 10, 2606.
- [59] H. Li, Y. Luo, P. Derreumaux, G. Wei, *Biophys. J.* **2011**, *101*, 2267.
- [60] N. Sharma, A. Top, K. L. Kiick, D. J. Pochan, Angew. Chem., Int. Ed. 2009, 48, 7078.
- [61] M. Sugiyama, A. Yurtsever, N. Uenodan, Y. Nabae, T. Fukuma, Y. Hayamizu, ACS Nano 2025, 19, 13760.
- [62] T. Fukuma, M. Kimura, K. Kobayashi, K. Matsushige, H. Yamada, Rev. Sci. Instrum. 2005, 76, 053704.

www.advancedsciencenews.com www.small-journal.com

- [63] J. L. Hutter, J. Bechhoefer, Rev. Sci. Instrum. 1993, 64, 1868.
- [64] A. Hjorth Larsen, J. Jørgen Mortensen, J. Blomqvist, I. E. Castelli, R. Christensen, M. Dułak, J. Friis, M. N. Groves, B. Hammer, C. Hargus, E. D. Hermes, P. C. Jennings, P. Bjerre Jensen, J. Kermode, J. R. Kitchin, E. Leonhard Kolsbjerg, J. Kubal, K. Kaasbjerg, S. Lysgaard, J.
- Bergmann Maronsson, T. Maxson, T. Olsen, L. Pastewka, A. Peterson, C. Rostgaard, J. Schiøtz, O. Schütt, M. Strange, K. S. Thygesen, T. Vegge, et al., J. Phys.: Condens. Matter 2017, 29, 273002.
- [65] J. Huang, A. D. MacKerell Jr, J. Comput. Chem. 2013, 34, 2135.
- [66] N. Michaud-Agrawal, E. J. Denning, T. B. Woolf, O. Beckstein, J. Comput. Chem. 2011, 32, 2319.